International Journal of Engineering & Technology, 7 (3.7) (2018) 541-545

International Journal of Engineering & Technology

Website: www.sciencepubco.com/index.php/IJET

Research paper



Proposal for Novel Supercontinuum Generated Photonic Crystal Fiber with High-Power for Ultrahigh-Resolution Optical Coherence Tomography

Feroza Begum[1*], Abul Kalam Azad[1], Emeroylariffion Abas[1], and Nianyu Zou[2]

[1]Faculty of Integrated Technologies, Universiti Brunei Darussalam, Brunei Darussalam
[2]School of Information Science and Engineering, Dalian Polytechnic University, Dalian, China
**Corresponding author E-mail: feroza.begum@ubd.edu.bn*

Abstract

We represent a novel photonic crystal fiber with high nonlinearity for optical coherence tomography application. The proposed highly nonlinear photonic crystal fibers different properties are computed based on finite difference method. Ultraflattened dispersion, small chromatic dispersion slope, large nonlinear coefficients, and very small confinement loss property are obtained for this designed highly nonlinear photonic crystal fiber. Moreover, the high power wideband super continuum spectrum and high longitudinal resolution of living tissue are achieved. Longitudinal resolution of living tissue is achieved 1.3 μm at center wavelengths 1.1 μm as well as 1.0 μm at center wavelengths 1.31 μm by applying picosecond pulse. Furthermore, the output power of 64.0 W at 1.1 μm center wavelength and 67 W at 1.31 μm center wavelength is demonstrated.

Keywords: *Photonic crystal fiber; supercontinuum spectrum; effective area; optical coherence tomography*

1. Introduction

The photonic crystal fibers (PCFs) have brought an advanced range of fibers with wider design space and manageable dispersion properties [1]. The highly nonlinear PCFs low dispersion wavelengths is possible to move from visible to near infrared for getting wideband supercontinuum (SC) with high peak power femtosecond lasers source [2]. It is possible to achieve extremely broad bandwidth SC sources from PCFs. The broad bandwidth SC spectrum is essential for optical coherence tomography (OCT) systems. Huang D, et al. was established OCT [3] at first and it is noninvasive medical imaging procedure. The internal cross-sectional images of biological tissue are obtained from high-resolution OCT. OCT imaging yields less dispersion, broad insertion and enhanced sensitivity around 1.0 and 1.3 μm wavelength. Around 1.0 μm wavelength is attractive in ophthalmology. Also, the wavelength around 1.3 μm is interesting in dentistry.

Commonly investigated broadband light sources like semiconductor-based superluminescent diodes (SLDs), femtosecond pulse laser sources and picosecond pulse laser source. The present OCT systems longitudinal resolution is depend on the light source optical bandwidth. Generally the SLDs optical bandwidth is 20 to 80 nm, longitudinal resolution is about 10 to 20 μm and low output power of 2 mW to 15 mW, which providing more detailed structural information [4, 5]. However, this achieved longitudinal resolution of SLD is not enough to detect single cells.

Up to 372 nm spectra centered at about 1.1 μm, 1.3 μm longitudinal resolution, about 50 mW of output power were generated by 110 fs Kerr-lens modelocked (KLM) Ti:sapphire oscillator [6]. A compact femtosecond Neodymium doped glass (Nd:glass) laser that provide ultrahigh resolution of 3.6 μm at 1.0 μm center wavelength [7]. A fiber-based, compact mode-locked ytterbium-doped (Yb-doped) laser permits longitudinal resolution of less than 1.6 μm at center wavelength 1.04 μm for ultrahigh-resolution OCT imaging [8]. An OCT light source connecting a LED and a near-infrared emitting glass ($1.0Yb_2O_3$-$4.0Nd_2O_3$-$47.0Bi_2O_3$-$47.0B_2O_3$-$1.0Sb_2O_3$) phosphor is used for center wavelength around 1.0 μm and obtained longitudinal resolution of 4.6 μm [9]. Neodymium-doped $Y_3Al_5O_{12}$-crystals (Nd:YAG) were investigated at around 1.0 μm center wavelength and analyze spectrum bandwidth is approximately 0.2 nm and output power of 1.3 W [10]. Generation a SC spectrum pumped with 200 fs Yb-doped fiber laser at a central wavelength of 1.07 μm is reported [11]. A FWHM bandwidth of 210 nm, longitudinal resolution of 3.7 μm and on sample output power of 10 mW are obtained by using a Cr^{4+}:forsterite laser source [12] at center wavelength 1.25 μm. SC generated single photonic crystal fiber with 85 fs pulse train compact Nd:Glass oscillator is demonstrated at center wavelength 1.3 μm in ultrahigh resolution OCT and it is reported 4.7 μm longitudinal resolution [13]. A Ge-doped PCF picosecond pulse laser were investigated at 1.31 μm center wavelength and obtained 6.1 μm of tooth enamel longitudinal resolution and 6.5 μm of dentin longitudinal resolution [14].

It is pointed out that still SLDs have suffered with low output power and narrow spectral bandwidth. Furthermore, femtosecond pulse based laser SC sources maintains better performance than that of SLDs. However, the cost of a femtosecond laser source is a big issue. Therefore, the low-cost, high power ultrabroadband light source is an essential issue for high performance OCT practically. The inexpensive picosecond SC laser light source which permits to implement economical wideband light source than that of expensive femtosecond SC light source.

Copyright © 2018 Authors. This is an open access article distributed under the Creative Commons Attribution License, which permits unrestricted use, distribution, and reproduction in any medium, provided the original work is properly cited.

In this research, we propose picosecond pulse based HN-PCF in around 1.0–1.4 μm wavelength OCT bands. It is obtaining wide bandwidth spectra, immense axial resolution of living tissue and large input power. According to numerically simulated result we have seen seen that the proposed highly nonlinear PCF exhibits nonlinear coefficients greater than 85 $[Wkm]^{-1}$ at 1.1 μm, 62 $[Wkm]^{-1}$ at 1.31 μm. The dispersion value is from zero to – 7.0 ps/(nm.km) remained between 1.06 μm to 1.4 μm wavelength. The dispersion slope value is ± 0.07 ps/(nm^2.km) changed within the wavelength region 1.06 μm to 1.40 μm. The lower confinement loss is 0.1 dB/km attained in the targeted wavelength spaces. On the other hand, longitudinal resolution is obtained 1.3 μm at 1.1 μm center wavelength and 1.0 μm at center wavelength 1.31 μm which are better than [4-14]. Moreover, power of 64 W at 1.1 μm center wavelength and 67 W at 1.31 μm center wavelength are achieved which are higher than [4-14].

2. Architecture of the Proposed PCF

In Figure 1, the architecture of the proposed highly nonlinear PCF (HN-PCF) is depicted. The 1st ring and 3rd ring air hole diameter is set d1, 2nd, 4th to 6th ring air hole diameter is set d, Λ is the center-to-center distance of two adjacent air holes, in this architecture. The cladding region periodicity in index-guiding PCF is unimportant to focus the light inside the core area. This designed principle is persuade the proposed HN-PCF to manage the chromatic dispersion slope and chromatic dispersion in broad range of wavelength. The cladding region regularity is changed by reducing the 1st and 3rd ring air hole diameter. The sizes of air hole are increased of remaining rings which are providing low confinement loss.

3. Simulation Method

The proposed HN-PCF different properties are computed by using full-vector finite difference method with anisotropic perfectly matched layer. The different properties include chromatic dispersion D(λ), chromatic dispersion slope, confinement loss Lc, mode effective area Aeff. Sellmeier equation is provided the material dispersion which is straight added in the chromatic dispersion calculation [15, 16]. Therefore, chromatic dispersion D(λ) correlate to the entire chromatic dispersion of the PCFs. Nonlinear coefficient γ is calculated with [17].

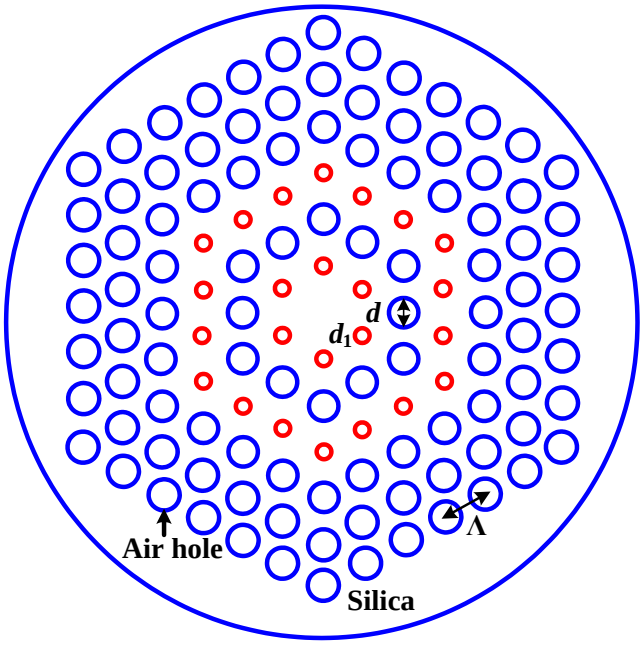
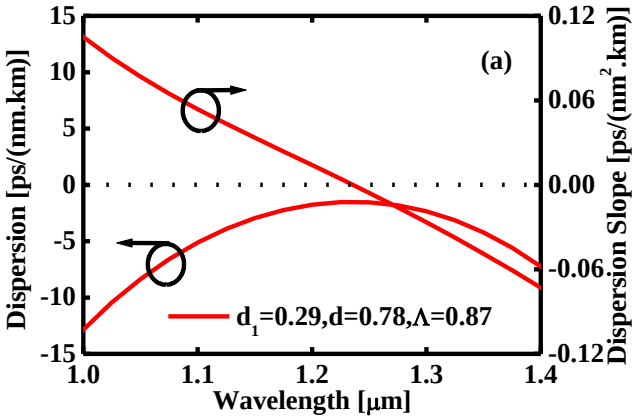


Figure 1: Architecture of the proposed six-ring highly nonlinear PCF.

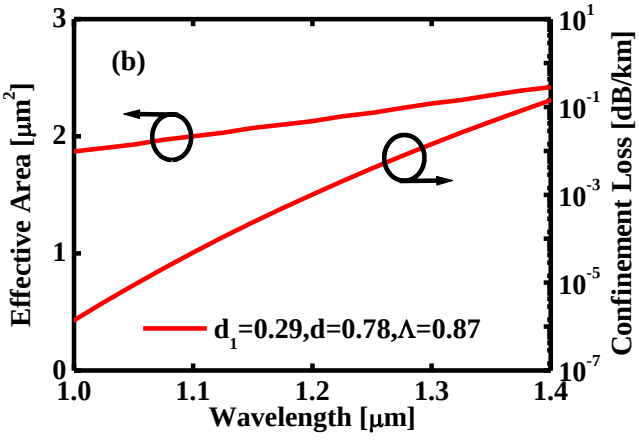
4. Results and Discussion

Figure 2(a) exhibits the chromatic dispersion and chromatic dispersion slope parameters of the proposed highly nonlinear PCF. And Figure 2(b) represents the effective mode area and confinement loss properties of the proposed HN-PCF. In this case, the air hole diameters are d1 and d, and pitch is Λ. The optimum chromatic dispersion is 0.0 – 7.0 ps/(nm.km) for the proposed highly nonlinear PCF between the wavelength range of 1.06 μm to 1.4 μm. The dispersion slope value is changed ± 0.07 ps/(nm2.km) in the wavelength range of 1.06 to 1.40 μm. In the targeted ranges wavelength, the low confinement loss of < 0.1 dB/km is achieved. The large nonlinear coefficient is obtained > 85 [Wkm]-1 at 1.1 μm and > 62 [Wkm]-1 at 1.31 μm.

For SC spectrum numerical calculation, nonlinear Schrödinger equation (NLSE) is applied [18]. The proposed HN-PCF numerically computed SC generation spectra is shown in Figures 3(a) and (b). In the proposed HN-PCF, the full width at half maximum (FWHM) sech2 input pulse 1.0 ps is considered for propagating through the fiber. In Figure 3, Raman scattering parameter TR is 3.0 fs. The incident pulse input power Pin is 64.0 W at 1.1 μm center wavelength λc and at 1.31 μm center wavelength λc 67.0 W. The computed β2 and β3 values are shown in Table 1 at 1.1 μm center wavelength and at 1.31 μm center wavelength. It is seen from Figure 3 that wide FWHM of SC spectrum of 435 nm and 291 nm are obtained at 1.31 μm center wavelength λc and at 1.1 μm center wavelength, respectively. From Table 1, it is seen that the power are 64 W and 67 W in two different center wavelengths; one is 1.1 μm and another one is 1.31 μm, respectively. This input powers of the applicable pulse are higher than [4-14].



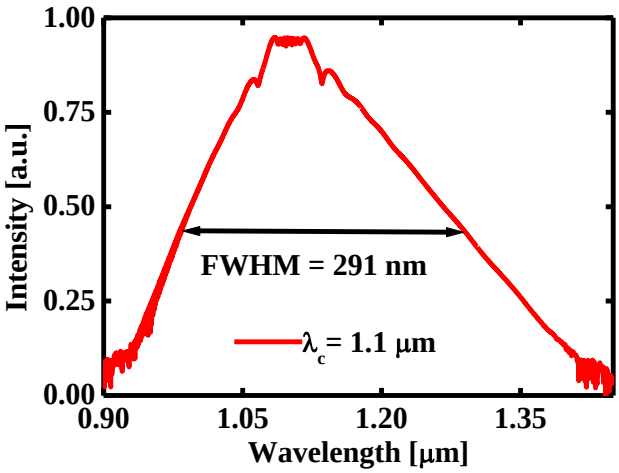
(a)



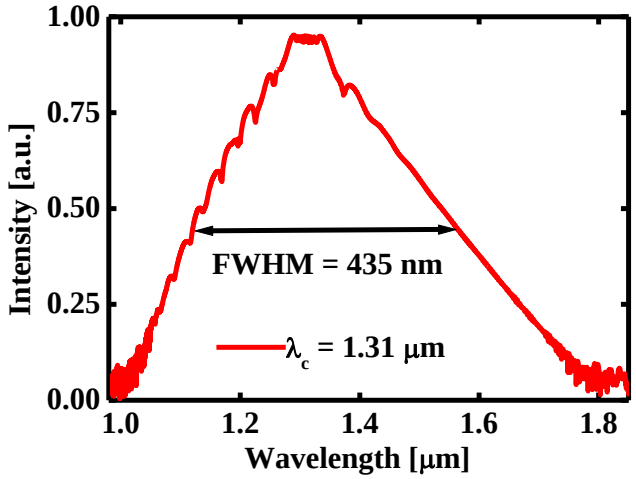
(b)

Figure 2: (a) Dispersion property and property of dispersion slope and (b) Property of effective area and property of confinement loss.

The air coherence length lc is expressed for a Gaussian spectrum by the formula [18]. In air, living tissue's longitudinal resolution, lr can be estimated by [18] after calculating coherence length lc. Because of lr is proportional with lc therefore the coherence length lc should be low value for ultrahigh-resolution OCT imaging. In our simulations, it is found that lc is 1.8 μm at 1.1 μm center wavelength as well as 1.7 μm at 1.31 μm center wavelength for the proposed HN-PCF. Therefore, the longitudinal resolution is obtained about 1.0 μm for dentin and 1.3 μm for ophthalmology. In table 1, the calculated lc and lr parameters are exposed. For this calculation, typical ntissue is considered 1.44 at 1.1 μm and 1.65 at 1.31 μm [19]. It is noted that these calculated lr parameters are better compared with recorded values in reference [4-14]. From the Table 1 calculated data, we observed that the best longitudinal resolution is obtained at center wavelength 1.31 μm between 1.1 μm center wavelength and at center wavelength 1.31 μm. Furthermore, it is noticed from table 1 that 6.0 m length fiber LF is obtained at 1.1 μm center wavelength which is shorter between two center wavelengths.



(a)



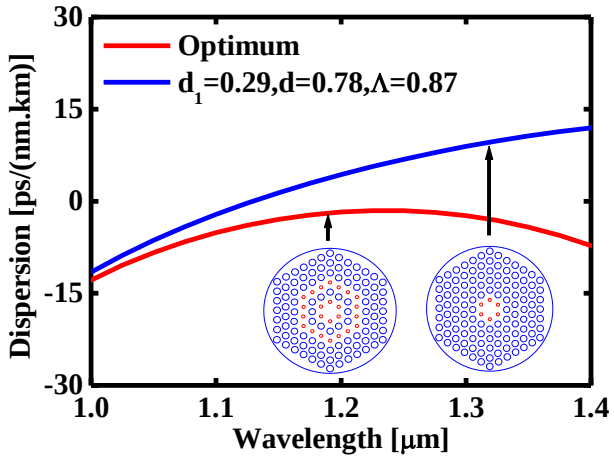
(b)

Figure 3: (a) SC spectrum at center wavelengths 1.1 μm and (b) SC spectrum at center wavelengths 1.31 μm.

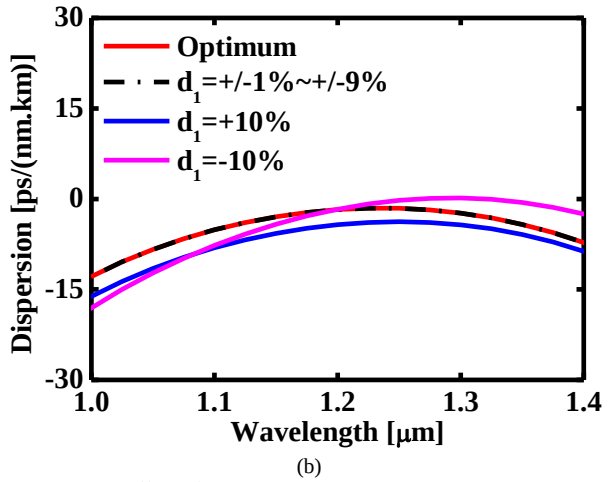
Table 1: Calculated parameters

Paramters	**λ_c = 1.1 [μm]**	**λ_c = 1.31 [μm]**
β_2 [ps^2/km]	3.1	2.5
β_3 [ps^3/km	0.006	-0.02
T_R [fs]	3.0	3.0
P_{in} [W]	64.0	67.0
L_F [m]	6.0	8.0
l_c [μm]	1.8	1.7
l_r [μm]	1.3	1.0

Figure 4 (a) shows the wavelength dependence chromatic dispersion properties. This graph shows the variation of chromatic dispersion after increasing third ring air hole diameter d1 from 0.29 μm to 0.78 μm. Here, first ring air hole diameters are d1 and the rest of air hole rings diameter are d. The proposed HN-PCF optimum chromatic dispersion curve is shown by solid red line when the first and third ring air hole diameters d1 = 0.29 μm, second, fourth to sixth-rings air hole diameters d = 0.78 μm, and Λ = 0.87 μm. It is seen from this chromatic dispersion graph that the obtained chromatic dispersion value is higher than the one of optimum chromatic dispersion value after increasing the third ring air hole diameter from 0.29 μm to 0.78 μm. It is clear from this result that to obtain flattened chromatic dispersion properties, the third ring air hole diameter has an enormous effect. In ref. [20], it has been mentioned that the fiber air hole diameter may vary of ± 1% during the fabrication process. For this reason, roughly ± 2% accuracy may be required for obtaining flattened dispersion. Moreover, in ref. [21], it is exhibited that the first ring air hole diameter is particularly important for maintaining the overall flattened chromatic dispersion. In consideration of this point, the first ring air hole diameter d1 is varied ± 1% to ± 10% from the optimum value of the proposed HN-PCF which is demonstrated in Figure 4(b).



(a)

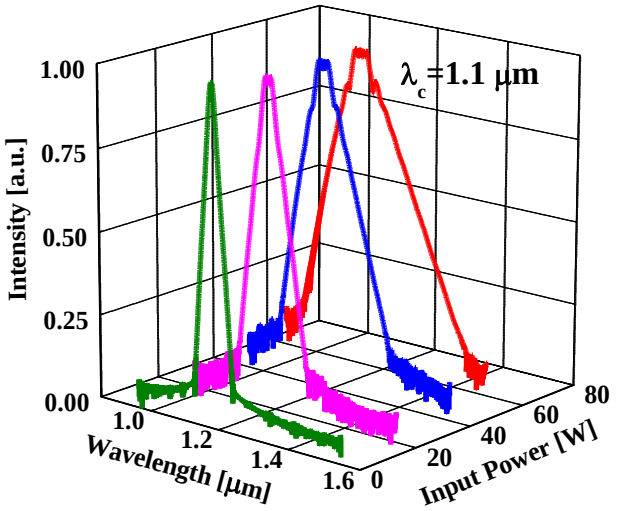


(b)

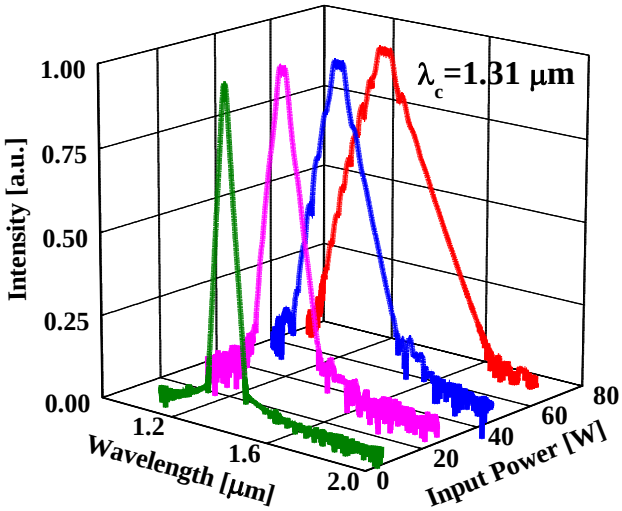
Figure 4: (a) Effect of third ring air hole diameter d_1 on the dispersion behavior with d_1 = 0.29 μm, d = 0.78 μm, and Λ = 0.87 μm, and (b) Chromatic dispersion variation after changing small air hole diameter d_1.

It is seen from the numerical results that the chromatic dispersion curves of the proposed HN-PCF is same with the optimum one until ± 9% variation of the diameter d1. A change in chromatic dispersion level is observed when the air hole diameter d1 is changed greater than that of ± 9%. It is observed from Fig. 4(b) that when d1 varies +10%, the flattened chromatic dispersion curves move below from the optimum one. Furthermore, from Figure 4(b), it has been recognized that while for -10% variation of d1 the chromatic dispersion curves shift downward direction with the optimum chromatic dispersion curve before around 1.2 μm wavelength and go to upward direction with the optimum

chromatic dispersion curve after around 1.2 μm wavelength. On the other hand, it is examined that zero dispersion wavelength is shifted in longer wavelength.



(a)



(b)

Figure 5: Optical intensity at center wavelengths (a) 1.1 μm and (b) 1.31 μm of the proposed HN-PCF in different input powers.

Figures 5 (a) and (b) reveals the proposed HN-PCF optical intensity in different input powers at center wavelengths 1.1 and 1.31 μm, respectively. It is seen that from figure 5 that intensity spectra are changing with input power, Pin. It is detected that intensity spectra are narrower with low input power and gradually broadening with high input power.

Finally, a comparison is provided between the proposed HN-PCF and some other reference papers properties for OCT applications which is represented in Table 2. Table 2 displays the value of different reference papers taking into account the spectrum FWHM bandwidth, longitudinal resolution and coherent power. All the values are taken at around 1.0 μm and 1.3 μm center wavelengths. From this Table 2 comparison, it should be pointed out that the proposed HN-PCF is achieved better longitudinal resolution and high power than other reference papers.

Table 2: Comparison between properties of the proposed HN-PCF and some other papers for OCT applications at around 1.0 μm and 1.3 μm wavelengths.

Laser light source	λ_c [μm]	$\Delta\lambda$ [nm]	l_r [μm]	Power [W]	Ref.
SLD	1.305	35	21	0.015	4
QD-SLD	1.19	80	7.8	-	5
Ti:sapphire	1.1	372	1.3	0.050	6
Nd:Glass	1.0	139	3.6	0.014	7
Yb-doped	1.04	30	1.6	0.140	8
Glass phosphor	1.014	98	4.6	0.001	9
Nd:YAG	1.064	0.2	-	1.3	10
Yb-doped	1.070	11	-	0.800	11
Cr^{4+}:forste-rie	1.250	210	3.7	0.010	12
Nd:Glass	1.3	156	4.7	0.048	13
Ge-doped PCF	1.31	75	6.5	-	14
ps pulse HN-PCF	1.1 1.31	291 435	1.3 1.0	64 67	Propos-ed PCF

5. Conclusion

In this research paper, the proposed HN-PCF different characteristics were calculated by using FDM in OCT window. On the other hand, SC spectra of the proposed PCF is studied depend on nonlinear Schrödinger equation. From simulation outcomes we observed that low dispersion slopes of ± 0.07 ps/(nm2.km), 0.0 – 7.0 ps/(nm.km) dispersion, greater than 85 [Wkm]-1 nonlinear coefficients at center wavelength 1.1 μm as well as larger than 62 [Wkm]-1 nonlinear coefficients at center wavelength 1.31 μm, and small confinement losses of < 0.1 dB/km could be achieved. Moreover, we observed that the high power wide supercontinuum spectrum at 1.1 μm center wavelength as well as at center wavelength 1.31 μm. The high axial resolution in living tissue of about 1.0 μm for dentin and 1.3 μm for opthamology could be obtained. From the architectural perspective, comparatively fewer analytical parameters are enforced for developing the proposed HN-PCF. For this reason, the architectural procedure would be more impressive and simple. This HN-PCF will be appropriate in various types of application including optical coherence tomography, wavelength division multiplexing sources, optical switching, optical regeneration, etc.

References

[1] Birks, T.A., et al., Endlessly single-mode photonic crystal fiber, Opt. Lett., 1997, 22: 961-963.
[2] Champert, P.-A., et al., White-light supercontinuum generation in normally dispersive optical fiber using original multi-wavelength pumping system, Opt. Express, 2004, 12: 4366-4371.
[3] Huang, D., et al., Optical coherence tomography, Science, 1991, 254: 1178-1181.
[4] Jung, E.J., et al., Spectrally-sampled OCT for sensitivity improvement from limited optical power, Opt. Express, 2008, 16: 17457-17467.
[5] Shibata, H., et al., Imaging of spectral-domain optical coherence tomography using a superluminescent diode based on InAs quantum dots emitting broadband spectrum with Gaussian-like shape, Japanese Jour. of Appl. Phys., 2015, 54: 04DG07-1-5.
[6] Wang, Y., et al., Ultrahigh-resolution optical coherence tomography by broadband continuum generation from a photonic crystal fiber, Opt. Lett. 2003, 28: 182-184.
[7] Bourquin, S., et al., Ultrahigh resolution real time OCT imaging using a compact femtosecond Nd:Glass laser and nonlinear fiber, Opt. Express, 2003, 11: 3290-3297.
[8] Lim, H., et al., Ultrahigh-resolution optical coherence tomography with a fiber laser source at 1 μm, Opt. Lett., 2005, 30: 1171-1173.
[9] Fuchi, S., et al., High Power and High Resolution Near-Infrared Light Source for Optical Coherence Tomography Using Glass Phosphor and Light Emitting Diode, Appl. Phys. Express, 2009, 2: 032102-1-3.
[10] Calmano, T., et al., Nd:YAG waveguide laser with 1.3 W output power, fabricated by direct femtosecond laser writing, Appl. Phys. B., 2010, 100: 131–135.

[11] Zaytsev, A., et al., Supercontinuum generation by noise-like pulses transmitted through normally dispersive standard single-mode fibers, Opt. Express, 2013, 21: 16056-16062.
[12] Herz, P.R., et al., Ultrahigh resolution optical biopsy with endoscopic optical coherence tomography, Opt. Express, 2004, 12: 3532-3542.
[13] Aguirre, A.D., et al., Continuum generation in a novel photonic crystal fiber for ultrahigh resolution optical coherence tomography at 800 nm and 1300 nm, Opt. Express, 2006, 14: 1145-1160.
[14] Namihira, Y., et al., Design of Highly Nonlinear Dispersion Flattened Hexagonal Photonic Crystal Fibers for Dental Optical Coherence Tomography Applications, Opt. Review, 2012, 19: 78–81.
[15] Zhu, Z., and Brown, T., Full-vectorial finite-difference analysis of microstructured optical fibers, Opt. Express, 2002, 10: 853-864.
[16] Begum, F., et al., Design and analysis of novel highly nonlinear photonic crystal fibers with ultra-flattened chromatic dispersion, Opt. Commun., 2009, 282: 1416-1421.
[17] Agrawal, G.P., 1995. Nonlinear Fiber Optics, Academic Press, San Diego, CA, 2nd Edition.
[18] Izatt. J.A., and Choma, M.A., Optical Coherence Tomography, Springer Publisher, 2008, pp. 47-72, Editors: Professor Dr. Wolfgang Drexler, Professor Dr. James G. Fujimoto.
[19] Ohmi, M., Ohnishi, Y., Yoden, K., and Haruna, M., In vitro simultaneous measurement of refractive index and thickness of biological tissue by the low coherence interferometry, IEEE Trans. on Biomedical Eng., 2000, 47: 1266-1270.
[20] Reeves, W.H., et al., Demonstration of ultra-flattened dispersion in photonic crystal fibers, Opt. Express, 2002, 10: 609-613.
[21] Poletti, F., et al., Inverse design and fabrication tolerances of ultra-flattened dispersion holey fibers, Opt. Express, 2005, 13: 3728-3736.